Asymmetric scattering and nonorthogonal mode patterns in optical microspirals

Jan Wiersig
Institut für Theoretische Physik, Universität Magdeburg, Postfach 4120, D-39016 Magdeburg, Germany

Sang Wook Kim
Department of Physics Education, Pusan National University, Busan 609-735, Korea

Martina Hentschel
Max-Planck-Institut für Physik komplexer Systeme, Nöthnitzer Straße 38, D-01187 Dresden, Germany
(Received 6 August 2008; published 6 November 2008)

Quasibound states in an open system do not in general form an orthogonal and complete basis. It is, however, expected that the nonorthogonality is weak in the case of well-confined states, except close to a so-called exceptional point in parameter space. We present numerical evidence showing that for passive optical microspiral cavities the parameter regime where the nonorthogonality is significant is rather broad. Here we observe almost-degenerate pairs of well-confined modes which are highly nonorthogonal. Using a non-Hermitian model Hamiltonian we demonstrate that this interesting phenomenon is related to the asymmetric scattering between clockwise and counterclockwise propagating waves in the spiral geometry. Numerical simulations of ray dynamics reveal a clear ray-wave correspondence.

DOI: 10.1103/PhysRevA.78.053809 PACS number(s): 42.25.−p, 42.55.Sa, 05.45.Mt, 42.60.Da

I. INTRODUCTION

Dielectric microdisks and spheres have been extensively studied due to the extraordinarily high quality factors (Q factors) achieved in such structures [1]. Such a merit is ascribed to the formation of so-called whispering gallery (WG) modes based on total internal reflection upon the surfaces of circular or spherical cavities [2]. However, these highly symmetrical shapes prohibit a directional light output, which is clearly disadvantageous for practical applications. An obvious solution is to break such symmetries by deforming the cavity shape [3–5]. The final goal in this direction is to obtain *unidirectional* output without degrading the high Q factor too much [6–10].

Chern *et al.* experimentally demonstrated unidirectional lasing from a spiral-shaped microcavity [6], see the sketch in Fig. 1. The maximum emission comes from the notch of the spiral at an angle ϕ of about $-35°$ [6,8,11] or some different angle [12–15]. The possible origins of these different results are discussed in Ref. [11]. It is clear that one characteristic feature of the spiral cavity plays a crucial role for the emission directionality: the chiral symmetry is broken so that the clockwise (CW) rotation is distinct from the counterclockwise (CCW) rotation [6]. Recently, the appearance of pairs of almost-degenerate modes with mainly CCW character but also small CW component has been observed [16]. Another characteristic feature of the spiral-shaped cavity is the existence of so-called quasiscarred modes [17,18]. These interesting modes seem to be localized along simple periodic ray trajectories. A careful analysis, however, shows that although these simple periodic trajectories do not exist in the conventional ray dynamics, they do exist in an augmented ray dynamics including Fresnel filtering [19].

Microcavities are open wave systems which are described not by Hermitian but by non-Hermitian operators [20], whose distinct properties are that their eigenvalues are in general complex and the eigenvectors are not orthogonal. The imaginary parts of the eigenvalues have the physical meaning of the decay rates of the modes. The modes of the spiral cavity can (in principle) be obtained by diagonalizing a non-Hermitian matrix so that they mutually form a nonorthogonal set. Another pronounced feature of the non-Hermitian matrix is the existence of exceptional points (EPs) in parameter space. At an EP (at least) two eigenvalues coalesce [21,22] and the corresponding two eigenvectors converge to each other so that the dimension of the eigenbasis of the non-Hermitian matrix is reduced [27]. It is known that not only does the nontrivial topology of complex eigenvalues around the EP exist [23], but also a relation to Berry's geometric phase which appears when external parameters are varied adiabatically [24–26]. Recently the non-Hermitian matrix and the EP have attracted much interest [28–32].

In this paper, we draw a connection from the appearance of almost-degenerate modes with mainly CCW character [16] to the broken chiral symmetry by the asymmetric scattering between CCW and CW traveling waves. We show that an effective two-by-two non-Hermitian matrix is extremely

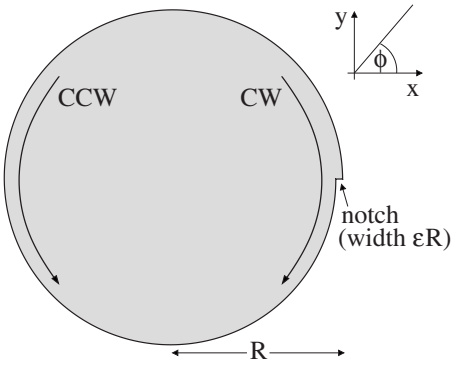

FIG. 1. Schematic top view of the spiral-shaped cavity. Clockwise (CW) and counterclockwise (CCW) traveling waves are indicated.

useful to understand the main characteristics of this relationship. When the effective transition rate from the CCW to the CW component, i.e., an off-diagonal element of the non-Hermitian matrix, vanishes, two eigenvalues of the matrix coalesce to form the EP, at which there exists only one eigenvector. The physical meaning of this is transparently revealed in the spiral cavities in the context of the time evolution of the scattering dynamics.

In Sec. II, we introduce the spiral cavity. Section III reports our numerical results on the properties of optical modes in this kind of cavity. In Sec. IV we introduce an effective non-Hermitian Hamiltonian to describe the nonorthogonality. The time evolution of waves is discussed in Sec. V. The ray-wave correspondence is the subject of Sec. VI. In Sec. VII we discuss the dependence of the mode properties on a shape parameter. A summary is given in Sec. VIII.

II. THE SYSTEM

Microdisk cavities are quasi-two-dimensional systems with piecewise constant effective index of refraction $n(x,y)$. In this case Maxwell's equations reduce to a two-dimensional scalar mode equation [33]

$$-\nabla^2\psi = n^2(x,y)\frac{\omega^2}{c^2}\psi, \tag{1}$$

with frequency $\omega=ck$, wave number k, and the speed of light in vacuum c. The mode equation (1) is valid for both transverse magnetic (TM) and transverse electric (TE) polarization. For TM polarization the electric field $\vec{E}(x,y,t)\propto(0,0,\mathrm{Re}[\psi(x,y)e^{-i\omega t}])$ is perpendicular to the cavity plane. The wave function ψ and its normal derivative are continuous across the boundary of the cavity. For TE polarization, ψ represents the z component of the magnetic field vector H_z. Again, the wave function ψ is continuous across the boundaries, but its normal derivative $\partial_\nu\psi$ is not. Instead, $n(x,y)^{-2}\partial_\nu\psi$ is continuous [33]. At infinity, outgoing wave conditions are imposed which results in quasibound states with complex frequencies ω in the lower half plane. Whereas the real part is the usual frequency, the imaginary part is related to the lifetime $\tau=-1/[2\ \mathrm{Im}\ \omega]$ and to the quality factor $Q=-\mathrm{Re}\ \omega/[2\ \mathrm{Im}\ \omega]$.

If the domain of interest is simply connected then the mode equation (1) can be written as the following eigenvalue equation:

$$\left(-\frac{c^2}{n^2}\nabla^2\right)\psi=\omega^2\psi. \tag{2}$$

In a closed cavity with vanishing wave function along the boundary the linear operator on the left-hand side is Hermitian. In the case of optical microcavities, however, the operator is non-Hermitian because of the outgoing wave conditions.

In polar coordinates (r,ϕ) the boundary of the spiral cavity is defined as

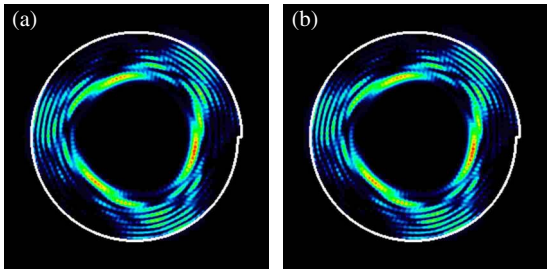

FIG. 2. (Color online) Calculated intensity $|\psi|^2$ of the nearly degenerate quasiscar modes 1 (a) and 2 (b).

$$r(\phi)=R\left(1-\frac{\varepsilon}{2\pi}\phi\right) \tag{3}$$

with deformation parameter $\varepsilon\geqslant 0$ and "radius" $R>0$ at $\phi=0$ as shown in Fig. 1. The radius jumps back to R at $\phi=2\pi$ creating a notch. Note that R is a trivial parameter which can be scaled away by using normalized frequencies $\Omega=\omega R/c=kR$. We are left with a one-parameter family of boundary shapes parametrized by ε. As in Ref. [16] we consider TE polarization, an effective index of refraction $n=2$ for silicon nitride, and, if not otherwise stated, the relative notch width $\varepsilon=0.04$.

III. MODE PROPERTIES

We use the boundary element method [34] to compute the spatial mode patterns $\psi(x,y)$ and the complex frequencies Ω. Figure 2 shows an interesting example, a pair of *nearly* degenerate modes, which are of quasiscar type [17,18]. One of these modes has $\Omega=41.4676-i0.03422$, i.e., a qualityfactor $Q_1=606$ and, if we assume $R=10\ \mu$m, a free-space wavelength $\lambda_1=1515.2$ nm. The other mode has $\Omega=41.4627-i0.03473$ corresponding to $\lambda_2=1515.38$ nm and $Q_2=597$. Not only the resonant wavelength and Q factor are very similar, but also the mode patterns depicted in Fig. 2. The question arises whether these numerical solutions really correspond to different modes. That this is indeed the case can be seen for instance in the far-field intensity patterns in Fig. 3. We can observe small oscillations with a phase difference of π superimposed on the common envelope.

Following Refs. [6,16] we analyze the mode pattern by expanding the wave function inside the cavity in cylindrical harmonics

$$\psi(r,\phi)=\sum_{m=-\infty}^{\infty}\alpha_m J_m(nkr)\exp(im\phi), \tag{4}$$

where J_m is the mth order Bessel function of the first kind. Positive (negative) values of the angular momentum index m correspond to CCW (CW) traveling-wave components. In Fig. 4(a) we can observe that for both modes the angular momentum distribution $|\alpha_m|^2$ is dominated by the CCW component, i.e., none of the two modes can be classified as CW traveling-wave mode. The tiny difference between the modes can be seen in Figs. 4(b) and 4(c). For negative angular momentum index both the real and the imaginary part of α_m

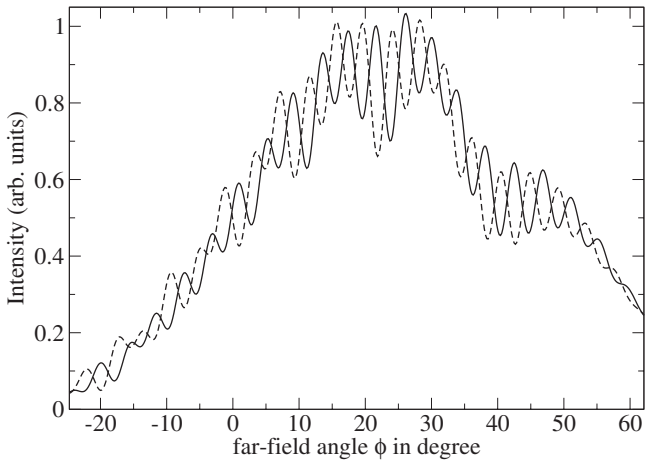

FIG. 3. Magnification of the computed far-field patterns of the modes in Fig. 2. The solid (dashed) line corresponds to mode 1 (2). For the definition of the far-field angle ϕ see Fig. 1.

have a different sign for the two modes which is nothing else than the phase difference of π observed in the far-field pattern. That means we can construct superpositions with $\alpha_m^{\pm}=(\alpha_m^{(1)}\pm\alpha_m^{(2)})/2$ being CW and CCW traveling waves, respectively, as can be seen in Fig. 4(d). Experimentally, the selective excitation of such traveling waves can be done by coupling light into the cavity via an attached waveguide [35]. It is important to emphasize that these superpositions are not eigenmodes of the cavity as they are composed of two modes with slightly different frequencies and Q factors.

The discussed properties of the angular momentum distributions are not restricted to quasiscar modes. Figure 5 depicts an example of a pair of "WG-like" modes in the same cavity. One mode has $\Omega=41.7166-i0.00207$, i.e., a quality factor $Q_1=10067$ and, if we again assume $R=10$ μm, a free-space wavelength $\lambda_1=1506.16$ nm. The other mode has $\Omega=41.7193-i0.00184$ corresponding to $\lambda_2=1506.06$ nm and $Q_2=11363$. Inspection of the angular momentum distributions in Fig. 6 shows qualitatively the same scenario as for the quasiscars, even though the asymmetry between CW and CCW components is much weaker.

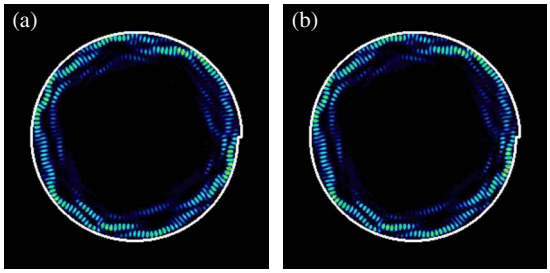

FIG. 5. (Color online) Calculated intensity $|\psi|^2$ of the nearly degenerate WG-like modes 1 (a) and 2 (b).

This kind of almost-degenerate modes in spiral-shaped cavities have already been observed in Ref. [16]. Here, we will discuss new features such as nonorthogonality of these modes and the implication on the time evolution of CW and CCW traveling waves in such cavities. To quantify the nonorthogonality we compute the normalized overlap integral of two modes ψ_1 and ψ_2 over the interior of the cavity $\mathcal{C}$,

$$S=\frac{|\int_{\mathcal{C}}dxdy\psi_1^*\psi_2|}{\sqrt{\int_{\mathcal{C}}dxdy\psi_1^*\psi_1}\sqrt{\int_{\mathcal{C}}dxdy\psi_2^*\psi_2}}. \tag{5}$$

For the quasiscar modes in Fig. 2 we find $S\approx 0.972$. This value close to unity means that the modes are nearly collinear. The overlap for the WG-like modes in Fig. 5 is $S\approx 0.481$, i.e., the nonorthogonality is weaker but still quite significant. Note that the overlap of modes from different pairs, i.e., one mode from Fig. 2 and one from Fig. 5, is numerically around 1% or below. That means, the modes are only pairwise nonorthogonal.

We have studied in total 60 modes in this cavity geometry within various frequency regimes and also for TM polarization. We always find that the modes come as strongly non-

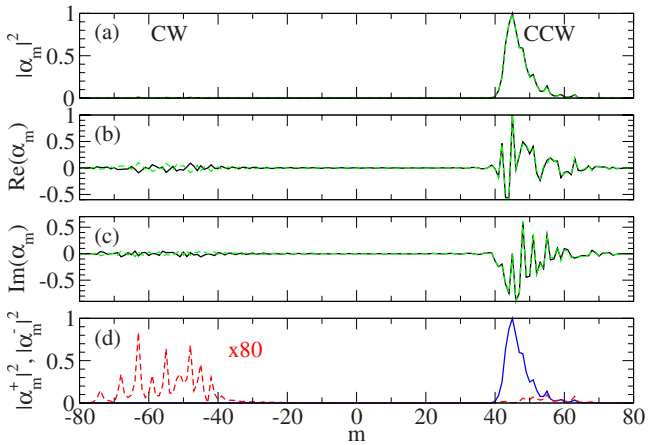

FIG. 4. (Color online) Angular momentum distributions $\alpha_m^{(1)}$ (solid line) and $\alpha_m^{(2)}$ (dashed) of quasiscar modes (see Fig. 2) normalized to 1 at maximum: (a) absolute value squared, (b) real, and (c) imaginary part. (d) Superpositions $\alpha_m^{+}=(\alpha_m^{(1)}+\alpha_m^{(2)})/2$ (solid) and $\alpha_m^{-}=(\alpha_m^{(1)}-\alpha_m^{(2)})/2$ (dashed, multiplied by a factor of 80).

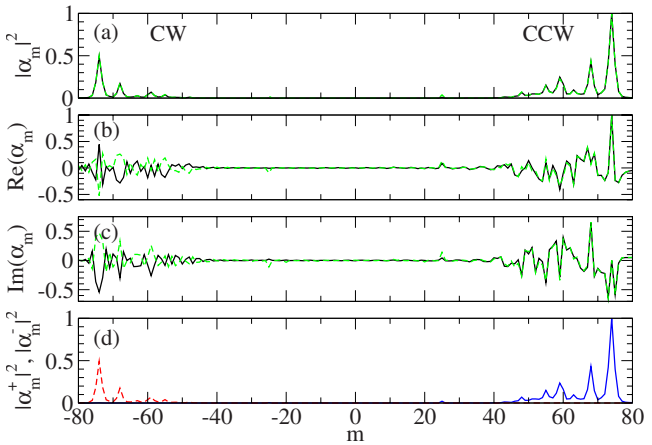

FIG. 6. (Color online) Angular momentum distributions $\alpha_m^{(1)}$ (solid line) and $\alpha_m^{(2)}$ (dashed) of WG-like modes (see Fig. 5) normalized to 1 at maximum: (a) absolute value squared, (b) real, and (c) imaginary part. (d) Superpositions $\alpha_m^{+}=(\alpha_m^{(1)}+\alpha_m^{(2)})/2$ (solid) and $\alpha_m^{-}=(\alpha_m^{(1)}-\alpha_m^{(2)})/2$ (dashed).

orthogonal pairs. We therefore conjecture that this is a generic property of optical modes in the spiral microcavity.

IV. EFFECTIVE NON-HERMITIAN HAMILTONIAN

In this section we demonstrate that the discussed behavior of the pairs of modes can be modeled by a simple toy model, the two-by-two non-Hermitian and nonsymmetric matrix

$$H = \begin{pmatrix} E_0 & 0 \\ 0 & E_0 \end{pmatrix} + \begin{pmatrix} \Gamma & V \\ \eta V^* & \Gamma \end{pmatrix}. \tag{6}$$

The eigenvectors of the first matrix on the right-hand side belong to the CCW and CW traveling waves with equal wave number $\sqrt{E_0} \in \mathbb{C}$ in the absence of any coupling between them. The first matrix suffices to describe the situation for the circular cavity ($\varepsilon=0$). In the general case of $\varepsilon>0$ the second matrix accounts for coupling effects which can be interpreted as scattering between CCW and CW traveling waves. The diagonal elements are given by the total scattering rates Γ which are assumed to be equal for simplicity. The off-diagonal element $V=|V|e^{i\delta} \in \mathbb{C}$ describes scattering from a CW traveling wave to the CCW traveling wave. The other off-diagonal element ηV^* describes scattering from a CCW traveling wave to the CW traveling wave. The latter scattering is assumed to be weaker, i.e., $0 \leqslant \eta < 1$, which is reasonable because of the geometry of the system, see Fig. 1. The complex eigenvalues of the matrix (6) are given by

$$E_\pm = E_0 + \Gamma \pm \sqrt{\eta}|V|. \tag{7}$$

The right eigenvectors turn out to be

$$\vec{\alpha}_\pm = \frac{1}{\sqrt{2}} \begin{pmatrix} 1 \\ \pm\sqrt{\eta} e^{-i\delta} \end{pmatrix}. \tag{8}$$

These eigenvectors directly explain the mode structure discussed in Sec. III. The weight of the first component (corresponding to CCW traveling waves) ~ 1 is much larger than that of the second component (corresponding to CW traveling waves) $\sim \eta$, cf. Figs. 4 and 6.

The two eigenvectors in Eq. (8) are nonorthogonal in the case of asymmetric scattering ($\eta \neq 1$),

$$\frac{|\vec{\alpha}_+^* \cdot \vec{\alpha}_-|}{|\vec{\alpha}_+||\vec{\alpha}_-|} = \frac{1-\eta}{1+\eta}. \tag{9}$$

Applying Eq. (9) to the pair of quasiscars in Fig. 2 with $S \approx 0.972$ yields $\eta^{-1} \approx 71$. This high degree of asymmetry in the scattering is consistent with the scaling factor of 80 in Fig. 4 using the connection to the mode structure in Eq. (8). In the case of the WG-like mode in Fig. 5 with $S \approx 0.481$ we obtain $\eta^{-1} \approx 2.8$. This lower degree of asymmetry in the scattering is in agreement with the fact that the CW component is only by a factor of about 2 smaller than the CCW component in Fig. 6.

The left eigenvectors of the matrix (6) are given by

$$\vec{\beta}_\pm = \frac{1}{\sqrt{2}} \left(1, \pm \frac{1}{\sqrt{\eta}} e^{i\delta} \right). \tag{10}$$

Left and right eigenvectors are orthogonal to each other, i.e., $\vec{\beta}_\pm \cdot \vec{\alpha}_\mp = 0$ and $\vec{\beta}_\pm \cdot \vec{\alpha}_\pm = 1$, as can be easily verified. Note that $\vec{\beta}_\pm^* \neq \vec{\alpha}_\pm$.

A remark is in order. In an open resonator the laser linewidth is increased with respect to the well-known Shawlow-Townes formula by the so-called Petermann factor K [36–38]. At an EP the Petermann factor is expected to diverge [39]. For the discussed non-Hermitian Hamiltonian the Petermann factor K is obtained as

$$K = \frac{\langle \beta_\pm | \beta_\pm \rangle \langle \alpha_\pm | \alpha_\pm \rangle}{|\langle \beta_\pm | \alpha_\pm \rangle|^2} = \frac{1}{4}\left(1 + \frac{1}{\eta}\right)(1+\eta), \tag{11}$$

which diverges as $\eta \to 0$. This property originates from the nonorthogonality of eigenstates of the non-Hermitian matrix. Interestingly, the Petermann factor K here depends solely on the degree of asymmetry η of the scattering between CW and CCW traveling waves.

V. TIME EVOLUTION OF CW AND CCW TRAVELING WAVES

The time evolution of waves is determined by the time-dependent Maxwell's equations which for a quasi-two-dimensional system can be written as

$$\ddot{\Psi} = -H\Psi. \tag{12}$$

Being of second-order this two-component differential equation has four independent solutions proportional to the eigenvectors of H. Two solutions $\vec{\alpha}_\pm e^{-i\sqrt{E_\pm}t}$ with positive frequency, $\mathrm{Re}\sqrt{E_\pm} > 0$, and two of the same kind with negative frequency. The solutions with negative frequency are not considered here separately as they come naturally into play when the real part of the wave function is taken to determine the z component of the magnetic field as

$$H_z(x,y,t) \propto \mathrm{Re}[\psi(x,y)e^{-i\omega t}] \tag{13}$$

$$\propto \frac{1}{2}[\psi(x,y)e^{-i\omega t} + \psi(x,y)^* e^{i\omega t}]. \tag{14}$$

From Eq. (8) it is clear that at $\eta=0$ we have an EP: the two right eigenvectors $\vec{\alpha}_\pm$ collapse into a single vector $(1,0)^T$, where the superscript T represents the transpose of the matrix. This eigenvector represents a pure CCW traveling wave. One can then ask the following questions: What is its physical implication? What happens if the initial state is chosen as $(0,1)^T$, i.e., normal to the eigenvector? To address these questions we rewrite the differential equation (12) in the following form by using $\Psi=(a,b)^T$:

$$\ddot{a} = -Ea - Vb, \tag{15}$$

$$\ddot{b} = -Eb, \tag{16}$$

where $E=E_0+\Gamma$. One solution is obviously

$$\Psi_1 = \begin{pmatrix} e^{-i\sqrt{E}t} \\ 0 \end{pmatrix}, \tag{17}$$

which exhibits an exponential decay in time, i.e. $|\Psi_1| \sim e^{-\gamma t}$, where $\gamma = -\mathrm{Im}\,\sqrt{E} > 0$ and $\mathrm{Re}\,\sqrt{E} > 0$. Note that the solution in Eq. (17) is proportional to the eigenvector $(1,0)^T$ of the Hamiltonian. One then expects $(0,1)^T$ could be another eigenvector. However, it is not true. When $(0,1)^T$ is chosen as the initial condition, one obtains

$$\ddot{a} + Ea = -Ve^{-i\sqrt{E}t}, \tag{18}$$

where the right-hand side comes from Eq. (16), which is independent of a. It is easy to see that

$$a(t) = \frac{V}{2i\sqrt{E}} te^{-i\sqrt{E}t} \tag{19}$$

is a solution of Eq. (18). Finally, one obtains

$$\Psi_2 = \begin{pmatrix} Vt/(2i\sqrt{E}) \\ 1 \end{pmatrix} e^{-i\sqrt{E}t}. \tag{20}$$

Note that Ψ_2 is not an eigenvector of H nor a simple harmonic function of time, but satisfies $(0,1)^T$ at $t=0$. Again there is an analog solution with negative frequency which is not considered here. One conclusion drawn from our analysis is that the differential equation (12) has two independent solutions (plus two with negative frequency) also at the EP, even though the eigenspace of the Hamiltonian H has only one dimension in this case.

The physical meaning of the two solutions (17) and (20) is clear in the spiral cavity. For Ψ_1 the state is initially prepared in the CCW traveling wave, so that it cannot make any transition to the CW since the corresponding transition rate is zero in the $\eta=0$ case. This is also intuitively acceptable because the CCW traveling wave experiences much less scattering than the CW traveling wave; see Fig. 1. For Ψ_2 the state is initially prepared in the CW traveling wave, and it exhibits the transition to the CCW leading to nonexponential time dependence. The scattering upon the notch gives rise to the transition from the CW to the CCW traveling wave so that the initial linear increase of the amplitude, see Eq. (20), comes into play. Such a nonexponential decay has been proposed in different context [40] and experimentally observed in a microwave cavity [31]. Slightly away from the EP with $\eta \gtrsim 0$ the two eigenvectors still have considerable overlap. One can therefore expect a similar behavior to occur also in the vicinity of the EP.

To confirm the discussed scattering scenario, we consider superpositions of modes which can be interpreted as pure CW or CCW traveling waves. As an example we take the quasiscar modes presented in Fig. 2. The modes evolve according to their complex frequencies $\omega_j = ck_j$ computed with the boundary element method. The first kind of superposition we consider is given by

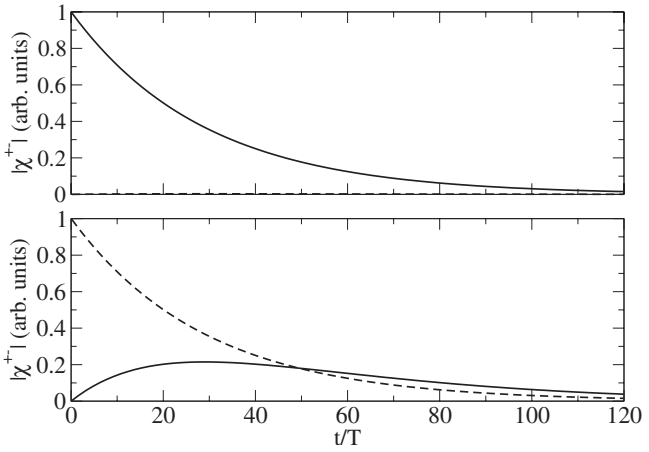

FIG. 7. Time evolution of CCW (solid lines) and CW (dashed) traveling waves. The traveling waves are superpositions of the quasiscar modes with frequencies Ω_1 and Ω_2 depicted in Fig. 2. The upper (lower) panel contains the dynamics starting with a pure CCW (CW) traveling wave. Time is measured in units of $T = 2\pi/\mathrm{Re}\,\Omega_1$.

$$\begin{pmatrix} \chi^+ \\ \chi^- \end{pmatrix} = \frac{1}{2}\begin{pmatrix} \alpha_1 \\ \alpha_2 \end{pmatrix} e^{-i\omega_1 t} + \frac{1}{2}\begin{pmatrix} \alpha_1 \\ -\alpha_2 \end{pmatrix} e^{-i\omega_2 t}. \tag{21}$$

For the coefficients α_j we choose as a rough approximation the maximal coefficients of the angular momentum distribution in Figs. 4(b) and 4(c): $\alpha_1 = 1$ and $\alpha_2 = 0.1 + i0.07$. For $t=0$ the superposition is purely CCW traveling as $\chi^+ = \alpha_1$ and $\chi^- = 0$. The upper panel of Fig. 7 shows the evolution of the superposition. We observe only a weak scattering into the CW component as it is expected from the two-by-two matrix (6) with small η. The second kind of superposition is

$$\begin{pmatrix} \chi^+ \\ \chi^- \end{pmatrix} = \frac{1}{2}\begin{pmatrix} \alpha_1 \\ \alpha_2 \end{pmatrix} e^{-i\omega_1 t} + \frac{1}{2}\begin{pmatrix} -\alpha_1 \\ \alpha_2 \end{pmatrix} e^{-i\omega_2 t}. \tag{22}$$

Initially, this superposition is a pure CW traveling wave since $\chi^+ = 0$ and $\chi^- = \alpha_2$. The lower panel of Fig. 7 shows the evolution of this superposition. Here we observe a strong scattering into CCW components with a linear increase of the amplitude as predicted by Eq. (20). In conclusion, the full mode calculation near the EP demonstrates very similar dynamical behavior as the effective non-Hermitian Hamiltonian at the EP. This clearly shows that at the EP nothing dramatic happens to the dynamics, even though the eigenspace of H collapses.

VI. RAY-WAVE CORRESPONDENCE

Our previous considerations have revealed that the peculiar time evolution of CCW and CW traveling waves plotted in Fig. 7 is related to the nonorthogonality associated with an EP. As the EP is an intrinsic wave phenomenon one would not expect to find a ray-wave correspondence in such a situation. Our numerical ray simulations, however, prove that this intuitive expectation fails. The upper panel of Fig. 8 has been computed by starting 10 000 rays uniformly at the boundary of the cavity with initial directions corresponding

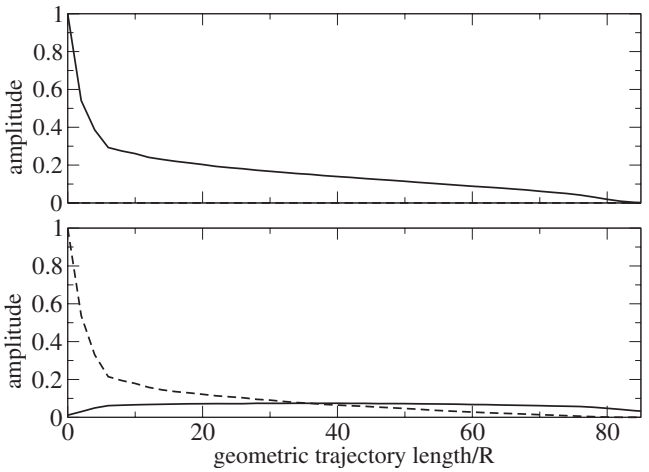

FIG. 8. Time evolution of amplitude (defined as square root of intensity in arbitrary units) corresponding to CCW (solid lines) and CW (dashed) propagating light rays. The upper (lower) panel shows the dynamics starting with a set of pure CCW (CW) propagating rays in full analogy to the wave dynamical considerations in Fig. 7. Time is proportional to the geometric length of ray trajectories.

to initially CCW propagation in the regime of total internal reflection. During the time evolution the rays can partially leave the cavity by refraction whenever the angle of incidence becomes smaller than the critical angle for total internal reflection. The transmission is given by Fresnel's laws. Moreover, rays can change their sense of rotation to CW propagation whenever they hit the notch. However, hitting the notch is very unlikely for CCW propagation rays as it is intuitively clear from Fig. 1. Therefore, practically all rays have completely left the cavity before they can change the sense of rotation. This is very different when the rays start initially in the CW sense of propagation as can be seen in the lower panel of Fig. 8. Here, rays can easily hit the notch and thereby change their sense of rotation. Comparison of the ray dynamics in Fig. 8 and the wave dynamics in Fig. 7 uncovers a striking correspondence. We believe that this unexpected ray-wave correspondence has two reasons: (i) In both cases the time evolution is governed by the asymmetric scattering between CW and CCW traveling components, and (ii) at the EP nothing special happens to the wave dynamics, despite the collapse of the eigenspace of H.

There are several facts which could explain the quantitative differences between the wave and ray dynamics: (i) The wavelength in the material λ/n is about $0.075R$ which is larger than the notch width $\varepsilon R=0.04R$. This is illustrated in Fig. 9. (ii) Diffraction at the corners is not included in the ray dynamics. We expect that for the WG-like modes diffraction at the corners can be important as the field intensity is larger at the corner than at the notch itself; see Fig. 9(b). Since diffraction at the corner is more uniform than direct scattering at the notch, see Ref. [41], diffraction explains why WG-like modes show less asymmetry (nonorthogonality) if compared to the quasiscar modes. (iii) The considered pair of modes are not uniformly distributed in phase space. (iv) For the coefficients α_j we have chosen only a rough estimation.

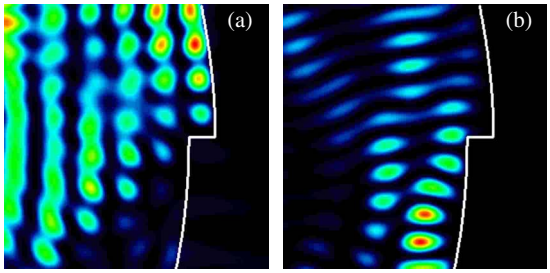

FIG. 9. (Color online) Magnification of the intensity pattern $|\psi|^2$ near the notch. (a) Quasiscar mode 2, as in the right panel of Fig. 2. (b) WG-like mode 2, cf. the right panel of Fig. 5.

VII. DEPENDENCE ON THE NOTCH WIDTH

In this section we discuss the dependence on the (relative) notch width ε. Let us first consider the trivial case $\varepsilon \to 0$, i.e., the circular cavity. Here, pairs of modes are exactly twofold degenerate. As a consequence the small decay rates $-\mathrm{Im}\,\Omega_j$ are equal and the level splitting $\Delta\Omega=|\mathrm{Re}\,\Omega_1-\mathrm{Re}\,\Omega_2|$ vanishes. The two modes with angular dependencies $\sim\sin(m\phi)$ and $\sim\cos(m\phi)$ are obviously orthogonal, i.e., the overlap integral S is zero.

Figure 10 shows the dependence of the decay rates, the level splitting, and the overlap integral as function of ε. As expected, the decay rates and the level splitting increase with increasing notch width ε. The overlap integral is close to unity, i.e., $1-S$ is small, in a broad parameter range. This robust behavior is an interesting finding since usually two parameters have to be carefully adjusted to an EP in order to obtain a significant effect. The degree of nonorthogonality increases as the scattering becomes more and more asymmetric with increasing notch width. At first glance, the fact that both nonorthogonality and level spacing increase with increasing ε seems to be in contradiction with our claim that the nonorthogonality is related to an EP where the level splitting is expected to go to zero. A closer inspection of Eqs. (7)

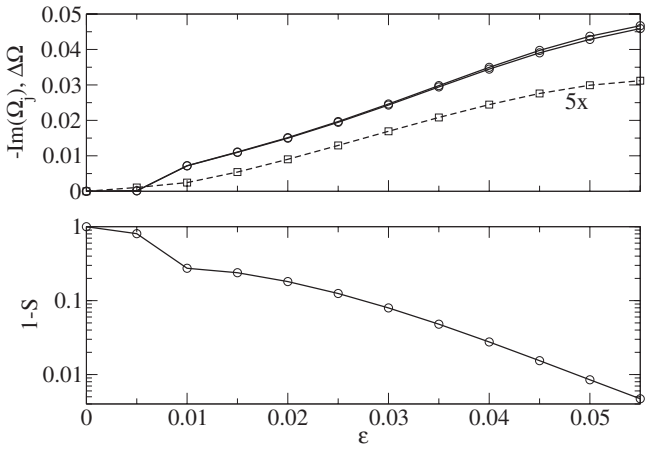

FIG. 10. The upper panel shows the individual decay rates $-\mathrm{Im}\,\Omega_j$ (circles) and the level splitting $\Delta\Omega=|\mathrm{Re}\,\Omega_1-\mathrm{Re}\,\Omega_2|$ (scaled by a factor of 5, squares) vs notch width ε. The corresponding overlap integral S computed from Eq. (5) is plotted in the lower panel. The lines are a guide to the eyes. The pair of modes for the particular case of $\varepsilon=0.04$ is the pair of quasiscars depicted in Fig. 2.

and (8), however, shows that there is no contradiction. According to Eq. (8) the EP is approached as $\eta(\varepsilon)$ is decreased. The level splitting, however, can increase as long as $|V(\varepsilon)|$ increases faster than $1/\sqrt{\eta(\varepsilon)}$. Roughly speaking, the strength of the scattering increases faster with the notch width than the asymmetry of the scattering.

Figure 10 clearly reveals the direct link between the almost-degenerate pairs in the spiral for finite ε and the exact degenerate pairs of modes with angular momentum number $m \neq 0$ in the circular cavity. This is another indication that the appearance of nonorthogonal pairs is a typical feature in the spiral cavity. Only very short-lived modes which belong to $m=0$ modes of the circle may not follow this scenario.

VIII. SUMMARY

We have demonstrated the appearance of highly nonorthogonal pairs of modes in optical microspiral cavities. With the help of a non-Hermitian Hamiltonian we have related this remarkable effect to exceptional points in parameter space. While usually two parameters have to be adjusted to come close to such a point, a broad interval of the natural shape parameter of the spiral geometry exhibits significant nonorthogonality. The physical mechanism behind this effect is the asymmetric scattering between clockwise and counterclockwise propagating waves. Simulations of ray dynamics have demonstrated a clear and unexpected ray-wave correspondence.

We believe that our work is of general importance for the understanding of open quantum and wave systems, in particular for microcavity lasers.

ACKNOWLEDGMENTS

We would like to thank T.Y. Kwon for discussions. Financial support by the DFG research group 760 "Scattering Systems with Complex Dynamics" and the DFG Emmy Noether Program is acknowledged. S.W.K. was supported by Pusan National University Research Grant.

[1] K. J. Vahala, Nature (London) **424**, 839 (2003).
[2] *Optical Processes in Microcavities*, edited by R. K. Chang and A. K. Campillo (World Scientific, Singapore, 1996).
[3] J. U. Nöckel and A. D. Stone, Nature (London) **385**, 45 (1997).
[4] C. Gmachl, F. Capasso, E. E. Narimanov, J. U. Nöckel, A. D. Stone, G. J. Faist, D. L. Sivco, and A. Y. Cho, Science **280**, 1556 (1998).
[5] A. D. Stone, Phys. Scr. **T90**, 248 (2001).
[6] G. D. Chern, H. E. Tureci, A. D. Stone, R. K. Chang, M. Kneissl, and N. M. Johnson, Appl. Phys. Lett. **83**, 1710 (2003).
[7] M. S. Kurdoglyan, S.-Y. Lee, S. Rim, and C.-M. Kim, Opt. Lett. **29**, 2758 (2004).
[8] M. Kneissl, M. Teepe, N. Miyashita, N. M. Johnson, G. D. Chern, and R. K. Chang, Appl. Phys. Lett. **84**, 2485 (2004).
[9] J. Wiersig and M. Hentschel, Phys. Rev. A **73**, 031802(R) (2006).
[10] J. Wiersig and M. Hentschel, Phys. Rev. Lett. **100**, 033901 (2008).
[11] M. Hentschel, T. Y. Kwon, M. A. Belkin, R. Audet, and F. Capasso (unpublished).
[12] T. Ben-Messaoud and J. Zyss, Appl. Phys. Lett. **86**, 241110 (2005).
[13] A. Fujii, T. Nishimura, Y. Yoshida, K. Yoshino, and M. Ozaki, Jpn. J. Appl. Phys., Part 2 **44**, L1091 (2005).
[14] A. Fujii, T. Takashima, N. Tsujimoto, T. Nakao, Y. Yoshida, and M. Ozaki, Jpn. J. Appl. Phys., Part 2 **45**, L833 (2006).
[15] R. Audet, M. A. Belkin, J. A. Fan, B. G. Lee, K. Lin, F. Capasso, E. E. Narimanov, D. Bour, S. Corzine, J. Zhu, and G. Höfler, Appl. Phys. Lett. **91**, 131106 (2007).
[16] J. Wiersig, Opt. Express **16**, 5874 (2008).
[17] S. Y. Lee, S. Rim, J. W. Ryu, T. Y. Kwon, M. Choi, and C. M. Kim, Phys. Rev. Lett. **93**, 164102 (2004).
[18] T. Y. Kwon, S. Y. Lee, M. S. Kurdoglyan, S. Rim, C. M. Kim, and Y. J. Park, Opt. Lett. **31**, 1250 (2006).
[19] E. G. Altmann, G. Del Magno, and M. Hentschel, Europhys. Lett. **84**, 10008 (2008).
[20] J. Okolowicz, M. Ploszajczak, and I. Rotter, Phys. Rep. **374**, 271 (2003).
[21] T. Kato, *Perturbation Theory of Linear Operators* (Springer, Berlin, 1966).
[22] W. D. Heiss, Phys. Rev. E **61**, 929 (2000).
[23] C. Dembowski, H. D. Gräf, H. L. Harney, A. Heine, W. D. Heiss, H. Rehfeld, and A. Richter, Phys. Rev. Lett. **86**, 787 (2001).
[24] C. Dembowski, B. Dietz, H. D. Gräf, H. L. Harney, A. Heine, W. D. Heiss, and A. Richter, Phys. Rev. Lett. **90**, 034101 (2003).
[25] C. Dembowski, B. Dietz, H. D. Gräf, H. L. Harney, A. Heine, W. D. Heiss, and A. Richter, Phys. Rev. E **69**, 056216 (2004).
[26] A. A. Mailybaev, O. N. Kirillov, and A. P. Seyranian, Phys. Rev. A **72**, 014104 (2005).
[27] W. D. Heiss, J. Phys. A **37**, 2455 (2004).
[28] J. Unterhinninghofen, J. Wiersig, and M. Hentschel, Phys. Rev. E **78**, 016201 (2008).
[29] J. Wiersig, Phys. Rev. Lett. **97**, 253901 (2006).
[30] H. Cartarius, J. Main, and G. Wunner, Phys. Rev. Lett. **99**, 173003 (2007).
[31] B. Dietz, T. Friedrich, J. Metz, M. Miski-Oglu, A. Richter, F. Schäfer, and C. A. Stafford, Phys. Rev. E **75**, 027201 (2007).
[32] J. P. Keating, M. Novaes, and H. Schomerus, Phys. Rev. A **77**, 013834 (2008).
[33] J. D. Jackson, *Classical Electrodynamics* (Wiley, New York, 1962).
[34] J. Wiersig, J. Opt. A, Pure Appl. Opt. **5**, 53 (2003).
[35] J. Y. Lee, X. Luo, and A. W. Poon, Opt. Express **15**, 14650 (2007).
[36] K. Petermann, IEEE J. Quantum Electron. **15**, 566 (1979).
[37] K. M. Frahm, H. Schomerus, M. Patra, and C. W. J. Beenak-

ker, Europhys. Lett. **49**, 48 (2000).
[38] H. Schomerus, K. M. Frahm, M. Patra, and C. W. J. Beenakker, Physica A **278**, 469 (2000).
[39] S.-Y. Lee, J.-W. Ryu, J.-B. Shim, S.-B. Lee, S. W. Kim, and K. An, Phys. Rev. A **78**, 015805 (2008).
[40] D. M. Cardamone, C. A. Stafford, and B. R. Barrett, Phys. Status Solidi B **230**, 419 (2002).
[41] F. Courvoisier, V. Boutou, J. P. Wolf, R. K. Chang, and J. Zyss, Opt. Lett. **30**, 738 (2005).